European Radiology (2019) 29:1607–1615
https://doi.org/10.1007/s00330-018-5714-6

CHEST

Differentiating between malignant and benign solid solitary pulmonary lesions: are intravoxel incoherent motion and diffusion kurtosis imaging superior to conventional diffusion-weighted imaging?

Qi Wan[1] · Ying-shi Deng[1] · Qiang Lei[1] · Ying-ying Bao[1] · Yu-ze Wang[1] · Jia-xuan Zhou[1] · Qiao Zou[1] · Xin-chun Li[1]

Received: 15 April 2018 / Revised: 1 August 2018 / Accepted: 9 August 2018 / Published online: 25 September 2018

Abstract

Objective To quantitatively compare the diagnostic values of various diffusion parameters obtained from mono- and biexponential diffusion-weighted imaging (DWI) models and diffusion kurtosis imaging (DKI) in differentiating between benign and malignant solitary pulmonary lesions (SPLs).

Methods Multiple b-value DWIs and DKIs were performed in 89 patients with SPL by using a 3-T magnetic resonance (MR) imaging unit. The apparent diffusion coefficient (ADC) of various b-value sets, true diffusivity (D), pseudo-diffusion coefficient (D*), perfusion fraction (f), apparent diffusional kurtosis (K_{app}), and kurtosis-corrected diffusion coefficient (D_{app}) were calculated and compared between the malignant and benign groups using a Mann-Whitney U test. Receiver-operating characteristic analysis was performed for all parameters.

Result The $ADC_{(0,\ 150)}$ values of malignant tumors were lower than those of the benign group ($p = 0.01$). The $ADC_{(0,\ 300)}$, $ADC_{(0,\ 500)}$, $ADC_{(0,\ 600)}$, $ADC_{(0,\ 800)}$, $ADC_{(0,\ 1000)}$, ADC_{total}, D, and D_{app} of malignant tumors were significantly lower than those of benign lesions (all $p < 0.001$). D*, f, and K_{app} showed no statistically significant differences between the two groups. ADC_{total} showed the highest area under the curve (AUC = 0.862), followed by $ADC_{(0,\ 800)}$(AUC = 0.844), $ADC_{(0,\ 600)}$(AUC = 0.843), D(AUC = 0.834), $ADC_{(0,\ 1000)}$(AUC = 0.834) and $ADC_{(0,\ 500)}$(AUC = 0.824), D_{app}(AUC = 0.796), and $ADC_{(0,\ 300)}$ (AUC = 0.773). However, the difference in diagnostic efficacy among these parameters was not statistically significant ($p > 0.05$).

Conclusion Intravoxel incoherent motion (IVIM) and DKI-derived parameters have similar performance compared with conventional ADC in differentiating SPLs.

Key Points

- *Mono- and biexponential DWI and DKI are feasible for differentiating SPLs.*
- *$ADC_{(0,\ \geq 500)}$ has better performance than $ADC_{(0,\ <500)}$ in assessing SPLs.*
- *IVIM and DKI have similar performance compared with conventional DWI in differentiating SPLs.*

Keywords Lung neoplasms · Solitary pulmonary nodule · Diffusion magnetic resonance imaging · Area under curve · Sensitivity and specificity

Abbreviations

ADC	Apparent diffusion coefficient
AUC	Area under curve
D	True diffusivity
D*	Pseudo-diffusion coefficient
D_{app}	Kurtosis corrected diffusion coefficient
DKI	Diffusion kurtosis imaging
DWI	Diffusion-weighted imaging
f	Perfusion fraction
IVIM	Intravoxel incoherent motion
K_{app}	Apparent diffusional kurtosis
ROC	Receiver operating characteristic
ROI	Region of interest
SPL	Solitary pulmonary lesions

✉ Xin-chun Li
xinchunli@163.com

[1] Department of Radiology, The First Affiliated Hospital of Guangzhou Medical University, Yanjiangxilu No 151., Guangzhou, China

Introduction

Lung cancer is one of the most common malignancies with the highest mortality [1]. Diagnosis and characterization of solitary pulmonary lesions (SPLs) is an important area of pulmonary medicine for clinical management. Although CT is a routine choice of chest imaging, it still has some limitations such as basing merely on a morphologic criterion and exposure to ionizing radiation. Magnetic resonance diffusion-weighted imaging (DWI), free of ionizing radiation and extraneous contrast media, allowed us to obtain information about the microscopic motion of water protons, which was indicative of changes at the cellular level [2]. DWI was introduced for pulmonary nodule assessment in 2008 [3, 4]. Since then, ADC, serving as a promising biomarker, has performed well in aspects of tumor detection and characterization and N-staging to treatment response assessment [5–7]. However, there is always concern that the ADC obtained from conventional monoexponential DWI could not accurately reflect the real diffusivity, owing to the influence of microcirculation [8].

It has been suggested that biexponential DWI or diffusion kurtosis imaging (DKI) might provide more accurate information about water diffusion [9, 10]. The intravoxel incoherent motion DWI (IVIM-DWI) calculated using a bi-exponential model could obtain diffusion (true diffusivity, D) and perfusion parameters (fraction of perfusion, f, and pseudo-diffusion parameter, D*) separately. IVIM of the oncology, either differentiating between benign and malignant tumors or monitoring treatment response, is a growing field of research. However, each IVIM-derived parameter might possess a different value in the differential diagnosis in various systems [11, 12]. The diffusion kurtosis models yield an estimate for excess kurtosis of the diffusion displacement probability distribution, accounting for the degree of the non-Gaussian pattern [13]. Although several preliminary studies of lung IVIM and DKI provided promising results, some inconclusive or conflicting results have also been published [10, 14]. Since mono- and biexponential DWI and DKI may demonstrate different aspects of tissue properties, it should be valuable to explore and compare their roles in the differentiation of solitary pulmonary lesions (SPLs).

To the best of our knowledge, no existing studies have quantitatively evaluated the diagnostic utilities of different diffusion models in differentiating SPLs. Therefore, the purpose of this prospective study was to quantitatively compare the potential of various diffusion parameters obtained from monoexponential, biexponential, and diffusion kurtosis models in the differentiation of SPLs.

Materials and methods

Patient population

This prospective study was approved by the local institutional review board. Written informed consent was obtained from each patient. A total of 196 consecutive patients with solid thoracic masses or nodules confirmed by computed tomography findings were referred to MR imaging between October 2015 and July 2017. The inclusion criteria were as follows: (1) lesions were measurable on computed tomography (CT) scan and (2) patients received no therapies or anti-inflammatory therapies at least 2 weeks before the MRI scan and lesions showed no shrinkage. The exclusion criteria were the following: (1) operations or biopsies were not performed (n = 21); (2) mediastinal lesions (n = 23); (3) multiple pulmonary lesions (n = 36); (4) masses or nodules have an air-containing area larger than 2/3 of the diameter (n = 8); (5) unsatisfactory imaging quality (n = 19). Finally, 107 patients were excluded, and a total of 89 patients (51 males and 38 females; age range, 23–77 years; mean age, 58.25 years) were included in the final cohort.

Pathologic assessment revealed 69 and 20 cases of malignant tumors and benign lesions, respectively, among the 89 SPLs. The malignancy group included 41 adenocarcinomas, 15 squamous carcinomas, 7 small cell carcinomas, 2 adenosquamous carcinomas, 1 combined small cell carcinoma (adenocarcinoma plus small cell carcinoma), 1 lymphoepithelioma-like carcinoma, 1 primary pulmonary synovial sarcoma, and 1 mucoepidermoid carcinoma. The benign tumor group included 5 focal pneumonias, 6 tuberculosis, 3 inflammatory granulomas, 3 sclerosing pneumocytomas, 2 hamartomas and 1 pulmonary sequestration.

Image data acquisition

All patients were examined with a 3.0-T MRI (Achieva, Philips Healthcare, Best, The Netherlands) using a body phase array coil (Philips Healthcare). Conventional MRI sequences include axial gradient echo T1-weighted (T1W) imaging and axial and coronal turbo spin-echo T2-weighted (T2W) imaging. Routine MR images were obtained during free-breathing. Axial T2WI was obtained with a repetition time/echo time of 998 /80 ms; section thickness, 5 mm; gap, 0.5 mm; field of view, 340 mm × 430 mm; NSA = 1; scan time, 24 s. Coronal T2WI was obtained with 1131/80 ms; section thickness, 5 mm; gap, 0.5 mm; field of view, 430 mm × 430 mm; NSA = 2; scan time, 27 s.

A multiple b-value DWI scan was acquired using a single-shot echo-planar imaging pulse sequence with free breathing. Parallel imaging was used, and fat was suppressed using spectral presaturation inversion recovery (SPIR). Fourteen b values from 0–1000 s/mm^2 were used (0, 5, 10, 15, 20, 25,

50, 80, 150, 300, 500, 600, 800, and 1000 s/mm^2), 1111/55 ms; section thickness, 3 mm; gap, 0.3 mm; field of view, 300 mm × 375 mm; NSA = 4; scan time, 7 min 17 s. DKI was performed by using three b values that ranged from 0 to 2000 s/mm^2 (0, 1000, 2000 s/mm^2) with six diffusion directions for every b value, 1084/66, section thickness, 4 mm; gap, 0.4 mm; field of view, 300 mm × 375 mm; NSA = 3; acquisition time, 4 min 5 s (Table 1).

Image data analysis and processing

The MR image data were processed using PRIDE software (Phillips Medical Systems). Multiple b-value DWI data were used to compute mono- and biexponential models. ADC_{total} and IVIM parameters (i.e., D, f, and D*) were calculated with mono- and biexponential fit models, respectively, using all 14 b values (0–1000 s/mm^2). The conventional ADC (i.e., ADC_{150}, ADC_{300}, ADC_{500}, ADC_{600}, ADC_{800}, ADC_{1000}) was calculated using two b values with b = 0 s/mm^2 and b = 150, 300, 500, 600, 800, and 1000 s/mm^2, respectively. DKI parameters (i.e., the apparent diffusional kurtosis, K_{app}, and the kurtosis corrected diffusion coefficient, D_{app}) were derived using three b values (0, 1000, 2000 s/mm^2). ADC values were calculated using monoexponential fit of signal intensity with the following equation [15]:

$$\frac{S(b)}{S_0} = \exp(-bADC)$$

For the biexponential IVIM model [16], the relationship between the DWI signal intensity and b factors can be expressed as:

$$\frac{S(b)}{S_0} = f \cdot \exp\left(-bD^*\right) + (1-f) \cdot \exp(-bD)$$

For the DKI model, DWI signal intensities at multiple b values were fitted with the following equation [17]:

$$\frac{S(b)}{S_0} = exp\left(-bD_{app} + \frac{1}{6}b^2D_{app}^2 \cdot K_{app}\right)$$

where S(b) is the signal intensity at different diffusion values, S_0 the signal intensity at b = 0 s/mm^2, f the fraction of perfusion, D the diffusion parameter representing pure molecular diffusion, and D* the pseudo-diffusion parameter representing incoherent microcirculation within the voxel. D_{app} is the kurtosis corrected diffusion coefficient, and K_{app} is a unitless parameter that represents the deviation of water motion from Gaussian diffusion.

After being transferred to a Philips workstation to generate two b-value ADC maps, the original DWI images were transferred to the post-processing software. Mono- and biexponential and kurtosis models were used to calculate the corresponding ADC_{total}, D, f, D*, K_{app}, and D_{app} pseudo color pictures. Least-squares fit was used for linear fitting with the monoexponential and DKI models, and IVIM data were fitted with the Levenberg-Marquardt nonlinear fitting algorithm. The region of interest (ROI) was manually drawn on the solid part of the lesion at the level of maximum transverse diameter, avoiding necrosis and hemorrhage by consensus of two experienced radiologists (Y.D. and Q.W. with 3 years and 7 years of magnetic resonance diagnostic experience, respectively) blinded to the pathologic results.

Statistical analyses

Data are presented as mean ± standard deviation (SD). IVIM and DKI parameters and ADC between malignant and benign groups were compared by Mann-Whitney U test. Receiver-operating characteristic (ROC) curve analysis was performed to evaluate the diagnostic performances and determine the optimal cutoff value of each parameter in predicting malignancy. Areas under the curves (AUCs) were compared using the

Table 1 Scanning parameters of magnetic resonance imaging

	T1WI	T2WI	Multiple b-value DWI	DKI
TR (ms)	10	998	1111	1084
TE (ms)	2.3	80	55	66
NSA	1	1	4	3
FOV (mm)	340 × 430	340 × 430	300 × 375	300 × 375
Slice thickness (mm)	5	5	3	4
Gap (mm)	0.5	0.5	0.3	0.4
B value	-	-	0, 5, 10, 15, 20, 25, 50, 80, 150, 300, 500, 600, 800, and 1000	0, 1000, 2000
Directions	-	-	3	6
Matrix	448 × 448	640 × 640	256 × 256	192 × 192
Scanning time	47 s	24 s	7 min 17 s	4 min 5 s

TR repetition time, *TE* echo time, *NSA* number of signals acquired, *FOV* field of view

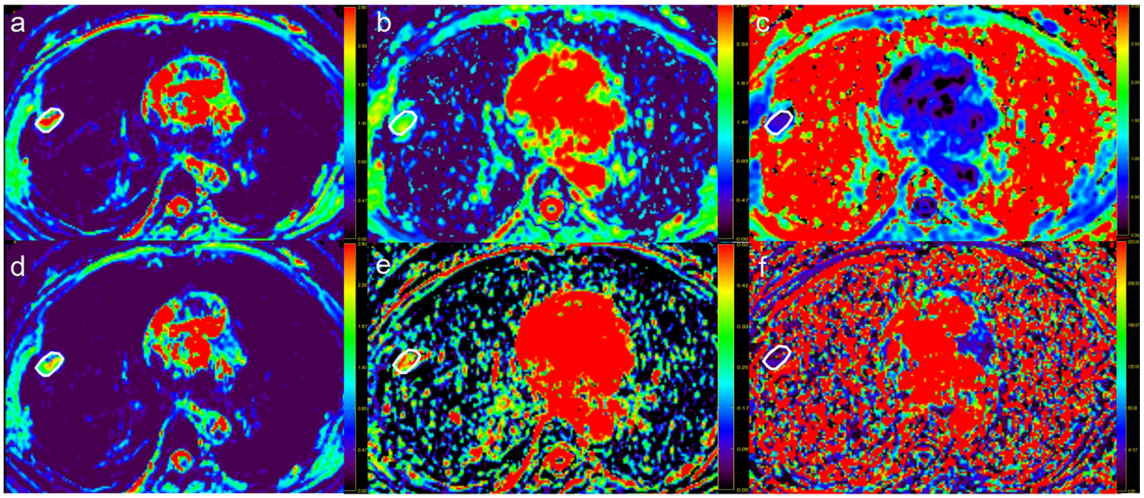

Fig. 1 Tuberculosis granuloma in the right lower lobe. In the lesion (**a**) the ADC_{total} map and (**b**) the D_{app} map show increased values. **c** The K_{app} map shows decreased values. **d** The D map, and (**e**) the f map show increased values. **f** The D* map shows decreased values. The "decreased" or "increased" values were described using the color in the middle of the bar as a reference

DeLong method. For pairwise comparisons of ROC curves, a Bonferroni-adjusted significance level of 0.017 (0.05/3) was used. Statistical analyses were performed with SPSS (version 19.0, IBM Corp., USA) and MedCalc software (version 15.2.2, Mariakerke, Belgium). The tests were two-tailed, and $p < 0.05$ was considered statistically significant.

Results

MRI appearance

The longest lesion diameters were in the range of 1.0–14.8 cm, with a mean of 4.2 cm. Figures 1, 2, 3, and 4 show the representative MR appearance on multiple diffusion images of two cases pathologically confirmed as benign and malignant lesion, respectively.

Diffusion parameters

ADC, IVIM, and DKI parameters of malignant and benign SPLs are shown in Fig. 5 and Table 2. The $ADC_{(0,\ 150)}$ of malignant tumors was lower than in the benign lesion group ($p = 0.01$). The $ADC_{(0,\ 300)}$, $ADC_{(0,\ 500)}$, $ADC_{(0,\ 600)}$, $ADC_{(0,\ 800)}$, $ADC_{(0,\ 1000)}$, ADC_{total}, D, and D_{app} of malignant tumors were significantly lower than in benign lesions (all $p < 0.001$). The difference of D*, f, and K_{app} between these two groups was not statistically different ($p > 0.05$).

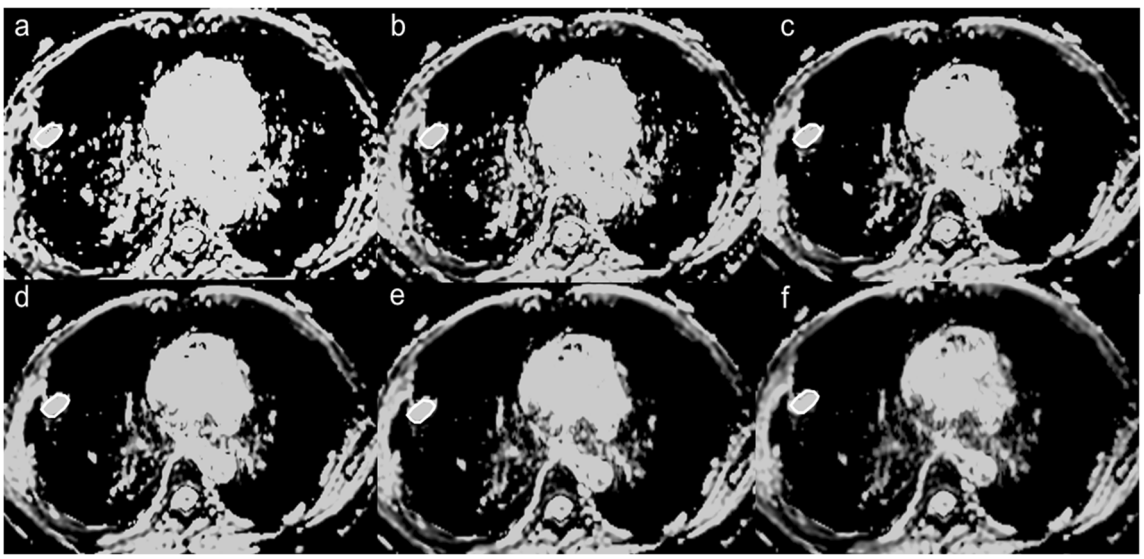

Fig. 2 The same patient as in Fig. 1. **a** $ADC_{(0,\ 150)}$ map. **b** $ADC_{(0,\ 300)}$ map. **c** $ADC_{(0,\ 500)}$ map. **d** $ADC_{(0,\ 600)}$ map. **e** $ADC_{(0,\ 800)}$ map. **f** $ADC_{(0,\ 1000)}$ map. The lesion continues to maintain a high level on ADC maps from low to high b values. $ADC_{(0,\ 150)} = 2.42 \times 10^{-3}$ mm^2/s, $ADC_{(0,\ 300)} = 2.38 \times 10^{-3}$ mm^2/s, $ADC_{(0,\ 500)} = 2.25 \times 10^{-3}$ mm^2/s, $ADC_{(0,\ 600)} = 2.23 \times 10^{-3}$mm^2/s, $ADC_{(0,\ 800)} = 2.12 \times 10^{-3}$ mm^2/s, $ADC_{(0,\ 1000)} = 1.92 \times 10^{-3}$ mm^2/s

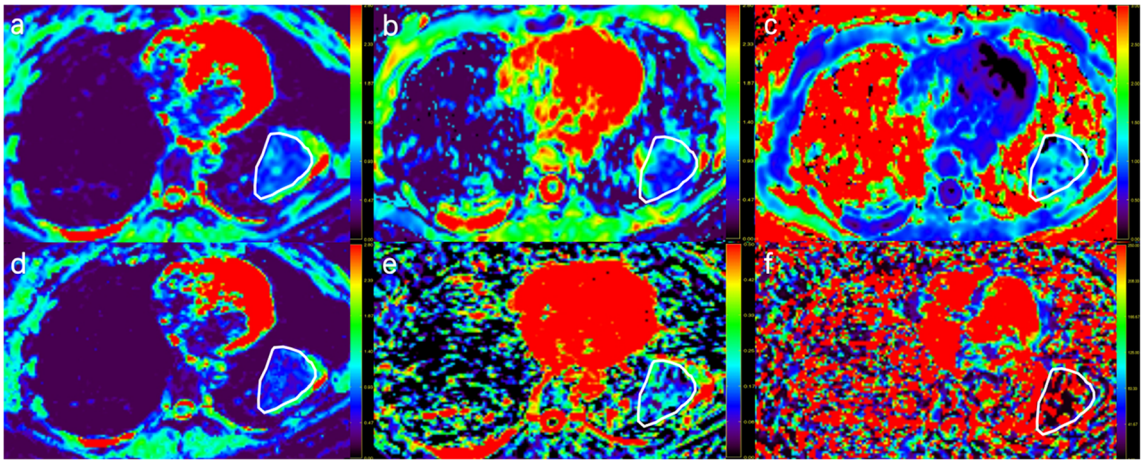

Fig. 3 Pulmonary lymphoepithelioma-like carcinoma in the left lower lobe. In the tumor (**a**), the ADC_{total} map and (**b**) the D_{app} map show decreased values. **c** The K_{app} map shows moderate to low values. **d** The D map shows decreased value. **e** The f map shows moderate to low values. **f** The D* map shows increased values. The "decreased" or "increased" values were described using the color in the middle of the bar as a reference

Diagnostic performance of multiple parameters

ROC curves of multiple parameters for predicting malignant SPLs were plotted in Fig. 6, and the corresponding diagnostic test characteristics are provided in Table 3. According to the ROC curve analysis, the AUC values of ADC_{total}, D, $ADC_{(0,150)}$ $ADC_{(0,\ 300)}$, $ADC_{(0,\ 500)}$, $ADC_{(0,\ 600)}$, $ADC_{(0,\ 800)}$, $ADC_{(0,\ 1000)}$, and D_{app} are 0.862, 0.834, 0.689, 0.773, 0.824, 0.843, 0.844, 0.834, and 0.796. For pairwise comparisons of ROC curves, ADC_{total} (p = 0.003), $ADC_{(0,\ 500)}$ (p = 0.008), $ADC_{(0,\ 600)}$ (p = 0.003), $ADC_{(0,\ 800)}$ (p = 0.004), and $ADC_{(0,\ 1000)}$ (p = 0.012) are better than $ADC_{(0,\ 150)}$ in diagnosing malignant SPLs. The difference in diagnostic efficacy among ADC_{total}, D, $ADC_{(0,\ 300)}$, $ADC_{(0,\ 500)}$, $ADC_{(0,\ 600)}$, $ADC_{(0,\ 800)}$, $ADC_{(0,\ 1000)}$, and D_{app} is not statistically significant.

Discussion

As a radiation-free alternative to CT for pulmonary nodule assessment, there is increasing interest in pulmonary magnetic resonance imaging. DWI, characterizing the restriction of random thermal motion of water molecules, is able to reveal tumor cellularity, which is beneficial for estimating and differentiating pulmonary nodules. However, the nodule detection rates with DWI are lower than the rates for other routine sequences, such as T2-weighted imaging [18]. Regier et al [19]

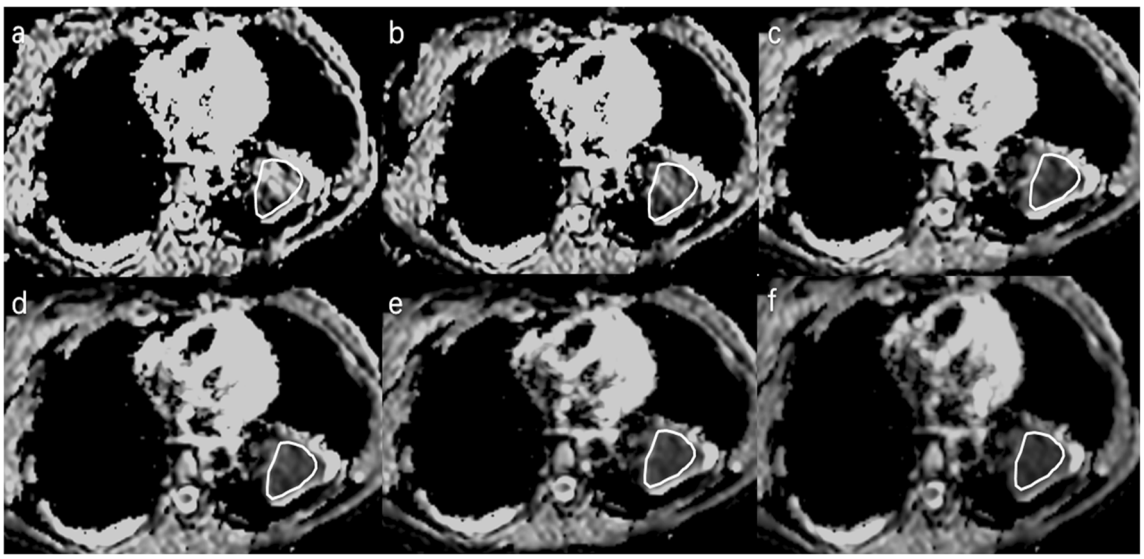

Fig. 4 The same patient as in Fig. 3. **a** $ADC_{(0,\ 150)}$ map. **b** $ADC_{(0,\ 300)}$ map. **c** $ADC_{(0,\ 500)}$ map. **d** $ADC_{(0,\ 600)}$ map. **e** $ADC_{(0,\ 800)}$ map. **f** $ADC_{(0,\ 1000)}$ map. The lesion shows descending value on ADC maps from low to high b values. $ADC_{(0,\ 150)} = 1.56 \times 10^{-3}$ mm^2/s, $ADC_{(0,\ 300)} = 1.17 \times 10^{-3}$ mm^2/s, $ADC_{(0,\ 500)} = 0.82 \times 10^{-3}$ mm^2/s, $ADC_{(0,\ 600)} = 0.73 \times 10^{-3}$ mm^2/s, $ADC_{(0,\ 800)} = 0.71 \times 10^{-3}$ mm^2/s, $ADC_{(0,\ 1000)} = 0.65 \times 10^{-3}$ mm^2/s

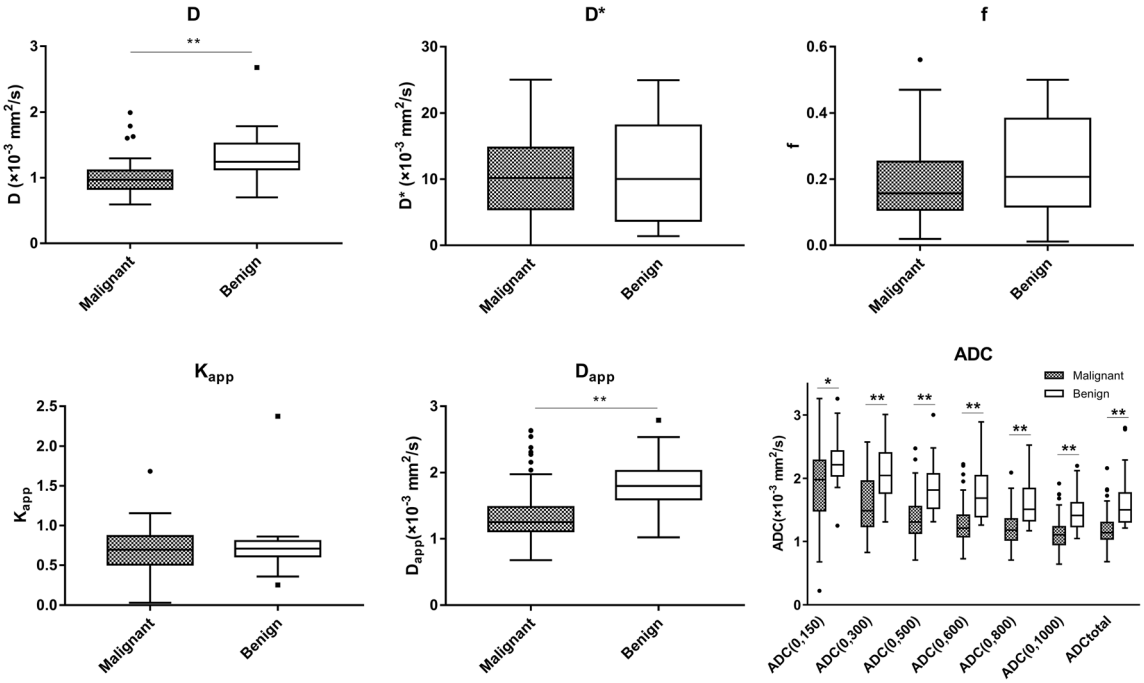

Fig. 5 Tukey boxplots of D, D*, f, ADC, D_{app}, and K_{app} values of malignant and benign solitary pulmonary lesions. $^{*}p = 0.01$, $^{**}p < 0.001$. Dots mean outliers. The Mann-Whitney U test was used for the comparison

found a sensitivity of only 43.8% with DWI for lung nodules ≤ 5 mm in diameter, which increased to 97% for nodules ≥ 10 mm. Therefore, currently DWI should be primarily used to assess lesions rather than nodule detection. According to a previous meta-analysis [20], most DWI studies on the lung choose a minimum of 10 mm as the inclusion criterion. In this study, the smallest lesion was 10 mm in diameter.

This study was conducted using free-breathing acquisition, consistent with most lung DWI studies. Although breath-holding or respiratory-triggered acquisitions can, to some extent, reduce the adverse effect of motion on DWI, they still have drawbacks, such as being challenging for some patients to perform (especially for those with COPD) and having much longer acquisition times (especially for IVIM) [14]. In contrast, free breathing is more versatile, and it is reported that there is no significant difference among the ADC measurements of these three methods [21].

Our study demonstrates that ADC, IVIM and DKI are clinically feasible and of value in differentiating between malignant and benign SPLs. Diffusion-related parameters, D, ADC, and D_{app}, possess relatively higher diagnostic accuracy compared with D*, f, and K_{app}. Malignant tumors have relatively lower numerical value in diffusion-related parameters compared with benign lesions, because malignant tumors tend to have a higher cell density and narrower extracellular space, thus leading to the limitation of the diffusion movement of water molecules.

Our study found that ADCs derived from b ≥ 500 s/mm^2 achieve better diagnostic performance compared with ADC derived from b < 500 s/mm^2. This may indicate that ADCs obtained from low b values (usually < 600 s/mm^2) tend to be unstable and more influenced by perfusion [22], which could lower the diagnostic performance. Nonetheless, if the b value is too high, it would increase the chance of distortion and susceptibility artifacts, especially in lung. In this study, the

Table 2 Diffusion parameters of malignant and benign solitary pulmonary lesions

Parameters	Malignant	Benign	*p* value
D	0.99 ± 0.25	1.27 ± 0.43	< 0.001
D*	11.10 ± 6.72	10.87 ± 8.10	0.709
f	0.18 ± 0.11	0.24 ± 0.14	0.118
K_{app}	0.67 ± 0.28	0.75 ± 0.41	0.810
D_{app}	1.36 ± 0.42	1.81 ± 0.41	< 0.001
ADC_{total}	1.19 ± 0.26	1.64 ± 0.46	< 0.001
$ADC_{(0,150)}$	2.26 ± 3.30	2.26 ± 0.41	0.01
$ADC_{(0,300)}$	1.58 ± 0.46	2.07 ± 0.45	< 0.001
$ADC_{(0,500)}$	1.38 ± 0.37	1.85 ± 0.39	< 0.001
$ADC_{(0,600)}$	1.28 ± 0.32	1.76 ± 0.42	< 0.001
$ADC_{(0,800)}$	1.21 ± 0.27	1.65 ± 0.39	< 0.001
$ADC_{(0,1000)}$	1.12 ± 0.26	1.48 ± 0.33	< 0.001

D true diffusivity, *D** pseudo-diffusion coefficient, *f* perfusion fraction, D_{app} kurtosis corrected diffusion coefficient, *ADC* apparent diffusion coefficient, K_{app} apparent diffusional kurtosis. Data are presented as mean ± standard deviation. Diffusion parameters between malignant and benign groups were compared by using Mann-Whitney U test. ADC, D, D_{app}, and D* are in units of ×10^{-3} mm^2/s

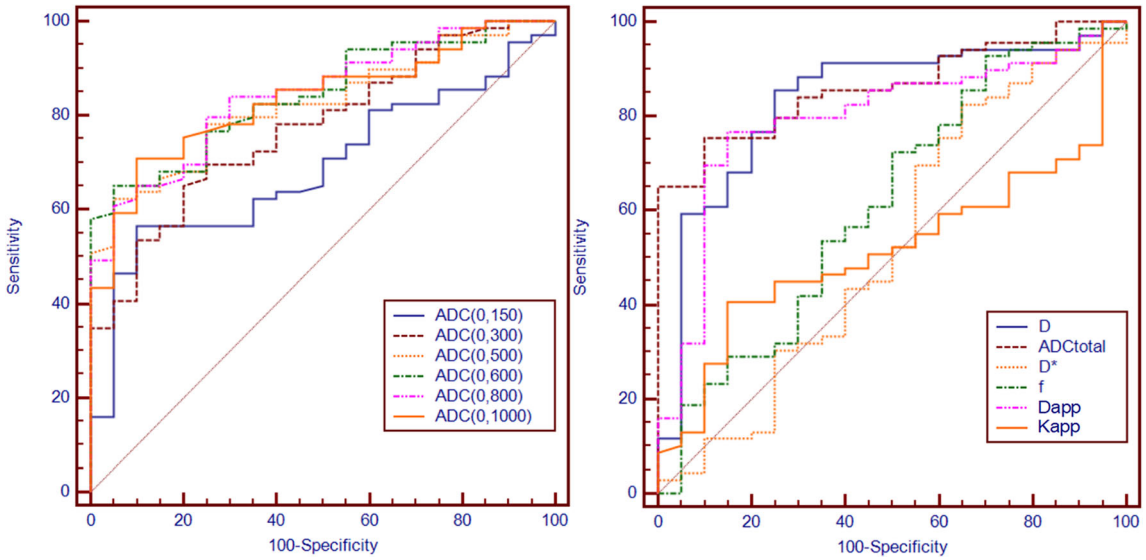

Fig. 6 Receiver-operating characteristic curves for D, D*, f, ADC, D_{app}, and K_{app} in distinguishing malignant from benign solitary pulmonary lesions

AUC of $ADC_{(0,\ 600–800)}$ was slightly higher than that of $ADC_{(0,\ 1000)}$. Although the difference is non-significant, we recommend obtaining two b-value DWI in lung with the maximum b value using 600–800 s/mm^2, taking both the imaging quality and diagnostic ability into account.

We noticed that D had the highest sensitivity, meanwhile $ADC_{(0,\ 500–800)}$ achieved the highest specificity. This means that D removal of the perfusion portion could be conducive to revealing the increased cellular density in malignancies and have a better performance in diagnosing malignant SPLs, while $ADC_{(0,\ 500\text{-}800)}$ sensitive to both diffusion and perfusion could be beneficial to synthetically reflect the pathologic conditions and have a relatively better performance in identifying non-malignant lesions. ADC_{total} seems like a compromise between them, possessing a maximum AUC in a non-significant manner. These findings suggest that the combination of D and ADC might be more accurate compared with these indices alone in clinical practice.

In this study, the perfusion-related values, D* and f, were not statistically different for the differentiation between benign and malignant SPLs, in line with previous studies [9, 23]. This may be due to the fact that the perfusion portion of benign and malignant nodules could overlap [9]. Furthermore, D* tends to be unstable and has a large standard deviation, which might also lead to a lower diagnostic potential. Nonetheless, in a study [14] with specific disease categories (including only lung cancer and inflammatory lesions), f was found significantly different between two groups. Therefore, further study with inflammatory lesions assessed separately may be needed.

The results of our study showed that the D_{app} of malignant groups was significantly lower than that of benign lesions, in accordance with Das [24]. However, unlike the previous study [24], we found that the K_{app} of malignant tumors was also lower than that of benign lesions with no statistical difference. This might suggest that benign lesions do not necessarily possess lower K_{app}. In this study, the K_{app} value of an

Table 3 Sensitivity and specificity of diffusion parameters at optimal cutoff values in differentiating malignant from benign solitary pulmonary lesions

Parameters	AUC	Cutoff value	Sensitivity (%)	Specificity (%)	+LR(%)	-LR(%)
D	0.834	1.138	85.51	75	3.42	0.19
D_{app}	0.796	1.484	76.81	85	5.12	0.27
ADC_{total}	0.862	1.296	75.36	90	7.54	0.27
$ADC_{(0,150)}$	0.689	2.013	56.52	90	5.65	0.48
$ADC_{(0,300)}$	0.773	1.734	65.22	80.0	3.26	0.43
$ADC_{(0,500)}$	0.824	1.423	62.23	95.0	10.43	0.50
$ADC_{(0,600)}$	0.843	1.305	65.22	95.0	13.04	0.37
$ADC_{(0,800)}$	0.844	1.238	60.9	95.0	12.17	0.41
$ADC_{(0,1000)}$	0.834	1.197	71.01	90	7.10	0.32

AUC area under ROC curve, *ADC* apparent diffusion coefficient, *D* true diffusivity, D_{app} kurtosis corrected diffusion coefficient, *95% CI* 95% confidence intervals, *+LR* positive likelihood ratio, *−LR* negative likelihood ratio

inflammatory lesion reaches as high as 2.37. This has not been reported before and might result from the relatively complex microenvironment, such as inflammatory cell infiltration, purulent exudate, or fibrous hyperplasia within the lesions. In addition, b-value selection might also account for the discordance. Technically, the highest b value using in DKI needs to reach > 1500 s/mm^2[13]. This study selected the 3b value with highest b = 2000 s/mm^2. Due to the scarcity of literature, the optimal b value selection for lung DKI remains unclear.

This study has some limitations. First, some other malignant (e.g., single metastasis, carcinoid, lymphoma) and benign (e.g., round atelectasis) lesions were not included in this study. The population of benign SPLs is relatively small, and the subtypes were not evaluated. Second, the ROIs were selected in the solid part on the largest slice instead of the entire tumors, which might lead to some selection bias owing to tumor heterogeneity. Third, some other promising diffusion models (e.g., diffusion basis spectrum imaging [25]) and quick acquisition techniques (e.g., slice accelerated diffusion imaging [26]) and were not used. In the future, the combination of different diffusion models with the detailed histologic characteristics should be investigated further in a larger study.

In conclusion, this study suggests that mono- and biexponential DWI and DKI are feasible and helpful in differentiating between malignant and benign SPLs. The conventional DWI using two b values with acceptable diagnostic efficiency and short scanning time can still be a convenient and effective choice for routine clinical application.

Funding This study has received funding from National Natural Science Foundation of China (81601457).

Compliance with ethical standards

Guarantor The scientific guarantor of this publication is Xinchun Li.

Conflict of interest The authors of this manuscript declare no relationships with any companies, whose products or services may be related to the subject matter of the article.

Statistics and biometry No complex statistical methods were necessary for this paper.

Informed consent Written informed consent was obtained from all subjects (patients) in this study.

Ethical approval Institutional Review Board approval was obtained.

Methodology
- prospective
- diagnostic study
- performed at one institution

References

1. Siegel RL, Miller KD, Jemal A (2017) Cancer statistics, 2017. CA Cancer J Clin 67:7–30
2. Le Bihan D, Iima M (2015) Diffusion magnetic resonance imaging: what water tells us about biological tissues. PLoS Biol 13: e1002203
3. Ohno Y, Koyama H, Onishi Y et al (2008) Non-small cell lung cancer: whole-body MR examination for M-stage assessment–utility for whole-body diffusion-weighted imaging compared with integrated FDG PET/CT. Radiology 248:643–654
4. Mori T, Nomori H, Ikeda K et al (2008) Diffusion-weighted magnetic resonance imaging for diagnosing malignant pulmonary nodules/masses: comparison with positron emission tomography. J Thorac Oncol 3:358–364
5. Cakmak V, Ufuk F, Karabulut N (2017) Diffusion-weighted MRI of pulmonary lesions: Comparison of apparent diffusion coefficient and lesion-to-spinal cord signal intensity ratio in lesion characterization. J Magn Reson Imaging 45:845–854
6. Koyama H, Ohno Y, Seki S et al (2015) Value of diffusion-weighted MR imaging using various parameters for assessment and characterization of solitary pulmonary nodules. Eur J Radiol 84:509–515
7. Koşucu P, Tekinbaş C, Erol M et al (2009) Mediastinal lymph nodes: assessment with diffusion-weighted MR imaging. J Magn Reson Imaging 30:292–297
8. Le Bihan D, Turner R (1992) The capillary network: a link between IVIM and classical perfusion. Magn Reson Med 27:171–178
9. Wan Q, Deng YS, Zhou JX et al (2017) Intravoxel incoherent motion diffusion-weighted MR imaging in assessing and characterizing solitary pulmonary lesions. Sci Rep 7:43257
10. Yuan J, Yeung DK, Mok GS et al (2014) Non-Gaussian analysis of diffusion weighted imaging in head and neck at 3T: a pilot study in patients with nasopharyngeal carcinoma. PLoS One 9:e87024
11. Marzi S, Stefanetti L, Sperati F, Anelli V (2016) Relationship between diffusion parameters derived from intravoxel incoherent motion MRI and perfusion measured by dynamic contrast-enhanced MRI of soft tissue tumors. NMR Biomed 29:6–14
12. Sumi M, Van Cauteren M, Sumi T, Obara M, Ichikawa Y, Nakamura T (2012) Salivary gland tumors: use of intravoxel incoherent motion MR imaging for assessment of diffusion and perfusion for the differentiation of benign from malignant tumors. Radiology 263:770–777
13. Rosenkrantz AB, Padhani AR, Chenevert TL et al (2015) Body diffusion kurtosis imaging: Basic principles, applications, and considerations for clinical practice. J Magn Reson Imaging 42:1190–1202
14. Deng Y, Li X, Lei Y, Liang C, Liu Z (2016) Use of diffusion-weighted magnetic resonance imaging to distinguish between lung cancer and focal inflammatory lesions: a comparison of intravoxel incoherent motion derived parameters and apparent diffusion coefficient. Acta Radiol 57:1310–1317
15. Lin M, Yu X, Chen Y et al (2017) Contribution of mono-exponential, bi-exponential and stretched exponential model-based diffusion-weighted MR imaging in the diagnosis and differentiation of uterine cervical carcinoma. Eur Radiol 27:2400–2410
16. Le Bihan D, Breton E, Lallemand D, Aubin ML, Vignaud J, Laval-Jeantet M (1988) Separation of diffusion and perfusion in intravoxel incoherent motion MR imaging. Radiology 168:497–505
17. Jensen JH, Helpern JA, Ramani A, Lu H, Kaczynski K (2005) Diffusional kurtosis imaging: the quantification of non-gaussian water diffusion by means of magnetic resonance imaging. Magn Reson Med 53:1432–1440

18. Meier-Schroers M, Homsi R, Schild HH, Thomas D (2018) Lung cancer screening with MRI: characterization of nodules with different non-enhanced MRI sequences. Acta Radiol. https://doi.org/10.1177/0284185118778870:284185118778870
19. Regier M, Schwarz D, Henes FO et al (2011) Diffusion-weighted MR-imaging for the detection of pulmonary nodules at 1.5 Tesla: intraindividual comparison with multidetector computed tomography. J Med Imaging Radiat Oncol 55:266–274
20. Shen G, Jia Z, Deng H (2016) Apparent diffusion coefficient values of diffusion-weighted imaging for distinguishing focal pulmonary lesions and characterizing the subtype of lung cancer: a meta-analysis. Eur Radiol 26:556–566
21. Cui L, Yin JB, Hu CH, Gong SC, Xu JF, Yang JS (2016) Inter- and intraobserver agreement of ADC measurements of lung cancer in free breathing, breath-hold and respiratory triggered diffusion-weighted MRI. Clin Imaging 40:892–896
22. Uto T, Takehara Y, Nakamura Y et al (2009) Higher sensitivity and specificity for diffusion-weighted imaging of malignant lung lesions without apparent diffusion coefficient quantification. Radiology 252:247–254
23. Yuan M, Zhang YD, Zhu C et al (2016) Comparison of intravoxel incoherent motion diffusion-weighted MR imaging with dynamic contrast-enhanced MRI for differentiating lung cancer from benign solitary pulmonary lesions. J Magn Reson Imaging 43:669–679
24. Das SK, Yang DJ, Wang JL, Zhang C, Yang HF (2017) Non-Gaussian diffusion imaging for malignant and benign pulmonary nodule differentiation: a preliminary study. Acta Radiol 58:19–26
25. Wang S, Peterson DJ, Wang Y et al (2017) Empirical comparison of diffusion kurtosis imaging and diffusion basis spectrum imaging using the same acquisition in healthy young adults. Front Neurol 8:118
26. Eichner C, Setsompop K, Koopmans PJ et al (2014) Slice accelerated diffusion-weighted imaging at ultra-high field strength. Magn Reson Med 71:1518–1525